Applications of Flow Control to Wing High-Lift Leading Edge Devices on a Commercial Aircraft

Arvin Shmilovich[1] and Yoram Yadlin[2]
Boeing Research and Technology, Huntington Beach, CA, 92647, USA

Paul Vijgen[3]
Boeing Commercial Aircraft, Everett, WA, 98204, USA

Rene Woszidlo[4]
Boeing Research and Technology, Hazelwood, MO, 63042, USA

Active flow control was applied to the leading edge region of a representative future short/medium-range twin-engine airplane to improve aerodynamic performance during high-lift operations. The study is aimed at enhanced lift over the practical angle of attack range, including stall, and at reduced drag. These benefits translate to airplane performance improvements, such as longer range or larger payload. Various flow control applications were explored using Computational Fluid Dynamics and the aerodynamic performance enhancements were benchmarked against the baseline configuration. The computational analyses are used to quantify aerodynamic benefits, as well as the input required for actuation. The results were used in a system integration study for identifying potential practical implementations, which are described in a companion paper. Combined with the integration analysis, the objective of this project is to identify the most promising flow control candidates that potentially provide material net airplane level enhancements using onboard fluidic sources. Depending on the implementation of active flow control, the current study indicates that up to 1.5% net improvement in L/D at takeoff and 4% increase in maximum lift during landing are potentially achievable, after accounting for factors of system integration.

Nomenclature

Parameters

A_{ref}	Wing reference area
A	Area vector
α	Angle of attack
C_D	Airplane drag coefficient
C_L	Airplane lift coefficient
C_{Lmax}	Maximum lift coefficient
C_μ	Total momentum coefficient, $\dot{m}u_j/(0.5\cdot\rho_\infty u_\infty^2 A_{ref})$
C_p	Pressure coefficient
C_q	Mass flow coefficient, $\dot{m}_j/(\rho_\infty u_\infty A_{ref})$

[1] Technical Fellow, Boeing Research and Technology, and AIAA Senior Member.
[2] Aerodynamics Engineer, Boeing Research and Technology, and AIAA Senior Member.
[3] Associate Technical Fellow, Boeing Commercial Aircraft, and AIAA Associate Fellow.
[4] Technical Lead Engineer, Boeing Research and Technology, and AIAA Associate Fellow.

L/D	Lift-to-drag ratio
Δ(L/D)	Percentage delta in lift-to-drag ratio, $100\cdot[(L/D)_{AFC}-(L/D)_{baseline}]/(L/D)_{baseline}$
M	Mach number
$\dot{m}$	Mass flow
P_{0in}	Total pressure at the actuator inlet
$P_{0\infty}$	Freestream total pressure
PR	Total pressure ratio, $P_{0in}/P_{0\infty}$
PT	Normalized total pressure, $P_0/P_{0\infty}$
Re	Reynolds number based on mean aerodynamic chord
ρ	Density
T_{0in}	Total temperature at the actuator inlet
$T_{0\infty}$	Freestream total temperature
TR	Total temperature ratio, $T_{0in}/T_{0\infty}$
U	Velocity vector
u_∞	Freestream velocity
x,y,z	Streamwise, spanwise and vertical coordinates, respectively

Subscripts

in	Actuator inlet
j	Actuation jet
th	Actuator throat
∞	Freestream
0	Stagnation

Abbreviations

1D	One dimensional
3D	Three dimensional
AFC	Active flow control
APU	Auxiliary Power Unit
CD	Convergent-divergent
CFD	Computational Fluid Dynamics
GD	Gas dynamics
IB, OB	Inboard, outboard
LE	Leading edge
NASA	National Aeronautics and Space Administration
OML	Outer mold line
RANS	Reynolds-Averaged Navier-Stokes
SA	Spalart-Allmaras turbulence model
WAI	Wing anti-ice

I. Introduction

The need for improved aerodynamic efficiency through the application of Active Flow Control (AFC) has motivated a number of studies over the years. Previous studies [1, 2] investigated potential benefits of reducing the cruise drag associated with modern high-lift systems. Although the performance benefits are tantalizing, that specific application dictates significant architectural changes to the aircraft, rendering it likely impractical for implementation in the next 15–20 years. Therefore, an intermediate application that matures and transitions AFC design and system capabilities in preparation for broader aircraft configuration changes is desired. A pathway toward more practical implementations may utilize localized AFC applications with limited architectural impact on the aircraft. The prospective use of localized AFC has become especially relevant after the successful demonstration of a full-scale AFC system in flight under a collaborative project between NASA and the Boeing Company [3]. In view of these findings, this study focuses on a set of applications targeting smaller regions of the airframe, yet are expected to offer meaningful net performance enhancements with manageable system integration.

Localized AFC applications to commercial transports may lead to substantial environmental and economic advantages for airplane operators. In particular, enhanced high-lift performance is one of the key objectives in aircraft design. Considering takeoff as an example, since the lift-to-drag ratio (L/D) is a major determinant of performance,

an increase in L/D allows for larger airplane payload, reduced runway length, and/or longer range, which translates to substantial economic advantages. Such benefits are illustrated by using several trade factors for a long range two-engine transport [4]:

- A 1.5% increase in maximum lift coefficient is equivalent to a 6,600 lbs increase in payload for a fixed approach speed.
- A 1% increase in takeoff L/D is equivalent to a 2,800 lbs increase in payload or a 150 nm increase in range.
- A 0.1 increase in lift coefficient at constant angle of attack is equivalent to reducing the approach attitude by one degree. As a result, the landing gear may be shortened for a savings in airplane weight of 1,400 lbs.

Motivated by these performance metrics, Boeing has recently initiated exploratory studies of new flow control concepts for high-lift applications using CFD. The new concepts include customary methods for reduced flow separation as well as unconventional approaches that target additional parameters for enhanced aerodynamic performance. This strategy offers a wider range of opportunities, improving the odds of identifying promising candidates for subsequent development. Promising approaches identified by Boeing for further development target different areas of the wing for AFC implementations. In one application, AFC is used to improve aerodynamic performance of ailerons, which are customarily deflected during high-lift operations. This application is the subject of a companion paper [5].

AFC can also be used at specific locations on the wing leading edge (LE) in conjunction with slats in order to enhance the performance of the high-lift system [6]. This paper describes a collaborative NASA/Boeing project that focuses on a variety of leading edge applications and it presents the computational simulation phase of the study. A representative configuration is used at the relevant flight conditions (takeoff and landing, sealed and gapped slats, etc.) with relatively modest configuration changes to accommodate AFC implementations. Various AFC layouts and actuation techniques are considered. By and large, the AFC methods are designed for the least amount of actuation power required for a specific design goal. The predicted aerodynamic data are used to establish airplane performance gains and to facilitate the integration phase of the study, which is described in a companion paper [7]. The entirety of this NASA/Boeing project is captured by four detailed reports [8–11].

II. Reference Aircraft and Computational Approach

This section describes the geometry of the Reference Aircraft, the computational strategy, the geometry setup and the grid system for the Reference Aircraft.

A. Geometry of Reference Aircraft

The Reference Aircraft was selected for the study of AFC. It represents a future, short/medium-range, twin-engine transonic airplane. The geometry definition, which includes fuselage, wing, Krueger flaps, slats, single-element flaps, nacelle/chine, aileron, etc., was adequate for CFD analysis. Detents of the high-lift elements were also available. Additional information on the structural layout, propulsion system, optional fluidic and power sources, and weights data for performance analysis and sizing, are used in the integration study [7].

High-lift geometries for takeoff and landing are considered. The takeoff configuration consists of a system of sealed slats and a Fowler flap system whose elements are deployed to the takeoff settings. At takeoff, the ailerons are symmetrically deflected to a nominal angle. The landing configuration employs a slotted slat system and flaps at appropriate detents. Customarily the ailerons are not deflected during landing. The high-lift system includes sealed Krueger flaps in the regions between the fuselage and engine pylons for both the takeoff and landing conditions.

B. Computational Method

The computational tool used for flow control is a modified version of the OVERFLOW code originally developed by NASA [12] and it forms the core process of Boeing's transport aircraft CFD in the context of AFC. OVERFLOW is based on the unsteady Reynolds-averaged Navier-Stokes (RANS) formulation for overset grid systems. The numerical procedure was modified to simulate flows for a family of flow control techniques [13, 14]. These include constant blowing, pulsed suction/blowing, swiveling jets (sprinkler), fluidic oscillators and traverse actuation. The simulation tool was generalized for large systems of actuators [2, 15, 16]. In most flow control applications, the computational domain contains the relevant physical region. It consists of the inner regions of the actuators and the external domain, enabling a complete simulation that captures the interplay amongst the actuator jets and the surrounding flow, irrespective of the actuation input. This coupling approach is adequate for any input pressure, whether the actuator flow is subsonic, choked, or intermittently subsonic/supersonic.

In this study, the second-order Roe upwind-differencing scheme is used with the ARC3D diagonalized Beam-Warming scalar pentadiagonal scheme on the right-hand side. The Spalart-Allmaras (SA) turbulence model has proven

robust in the context of the highly separated flows and is used for the simulation cases presented here. The time stepping scheme is second order as demonstrated in the framework of AFC using a system with multiple actuators [15]. The numerical procedure has been extensively validated for numerous applications of AFC [15, 17] through both wind tunnel settings and flight testing [16]. The validation studies include the characterization of flow control devices for the range of practical actuation parameters, as well as the performance of airplanes equipped with large systems of actuators. A more pertinent validation is described in the companion paper [5].

C. Geometry Setup and Grid System

A set of geometric simplifications were introduced to the Reference Aircraft in order to allow for quicker computational turnaround without compromising the modeling of the flow control effects. The horizontal tail, the landing gear and the brackets of the LE devices, as well as the flap track fairings are excluded from the computational model. Flow-through engines are used in all the simulations presented here. The wing is rigid, and therefore, no aeroelastic effects are accounted for in the simulations. No yaw conditions are considered here, so the simulations are performed on half of the airplane and assuming a vertical plane of symmetry.

The geometry of the surface grids in Fig. 1 shows close views of the slat in the takeoff positions. The single-element flap is deflected to 20°. The aileron is deflected to a nominal angle of 7.5° as customarily used during contemporary takeoff procedures. The wing LE consists of a sealed Krueger flap inboard of the engine station. Outboard of the engine there are four slat elements, which are in the sealed position. In the majority of the simulations, the slats are treated as a continuous element, unless otherwise noted.

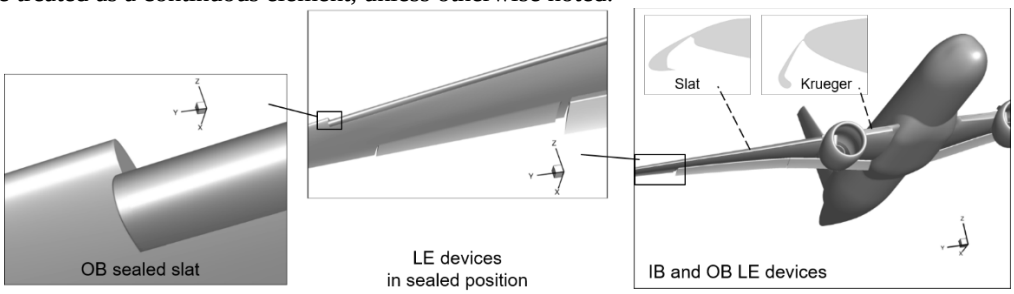

Fig. 1 Takeoff geometry used in the modeling of flow control in the wing leading edge region.

III. Results with Localized Leading Edge AFC Concepts

AFC concepts for high-lift applied to the wing LE devices and the nacelle/pylon/wing are explored for both takeoff and landing conditions. The approaches target reduced drag and enhanced lift over the range of practical angles of attack, including stall. Another objective is to provide solutions for the integration of the high-lift system with high-by-pass-ratio engines. A set of optional AFC layouts were analyzed and promising candidates were identified based on improved aerodynamic performance relative to the input required for actuation. Throughout this study, the new AFC concepts were developed while continually taking into consideration aspects of integration. The practicality of the AFC implementations is assessed in the integration study in a companion paper [7].

The flow control approaches considered here use constant blowing. Based on Boeing's experience, actuation based on constant blowing is also a suitable proxy for unsteady actuation that, depending on actuation parameters, could potentially provide higher efficiencies.

A. AFC in Leading Edge Region

A method that aims at improved L/D at takeoff by applying flow control at the leading edge devices is investigated here. In one example, AFC is used in conjunction with the deployed slats, which was the subject of a previous study [6]. Subsequent to that study, Boeing embarked on a follow-on internal investigation to refine the AFC approach. A set of actuators was embedded within the slat cove as an integral part of the high-lift system in order to enhance its performance and efficiency. During takeoff, the slats are deployed and the actuators are simultaneously activated. The system of air jets alters the flow recirculation within the cavity formed by the slat and main wing element. This flow mechanism results in the reduction of total airplane drag. This is an unconventional application of flow control, which is customarily used for reduced flow separation.

Computational assessments are used to investigate AFC applications in the slat cove as well as other related flow control concepts at the wing LE. Actuation modes and parametric sensitivities are established for the Reference

Aircraft. The primary objective is to identify promising AFC approaches and preferred layouts that yield improved takeoff L/D and C_{Lmax} while using low actuation input.

1. Proximity to Fluidic Sources

The proximity to potential fluidic sources is an important factor in the design of the AFC system. Therefore, considerations with regard to their potential availability is in order. Figure 2 presents a schematic layout of the Reference Aircraft, identifying the LE devices at which AFC is being considered. Flow control is considered for the set of slats outboard of the engine strut (pylon). Air ducting is available in the strut region, where potential sources include engine bleed. Also, an existing APU line at the engine station could be tapped into. Another potential source is the hot air of wing anti-ice (WAI) used in slats 3 and 4, and might offer AFC efficiencies associated with high temperature supply [18, 19]. Finally, compressors might be embedded at the wing LE for localized treatment with flow control.

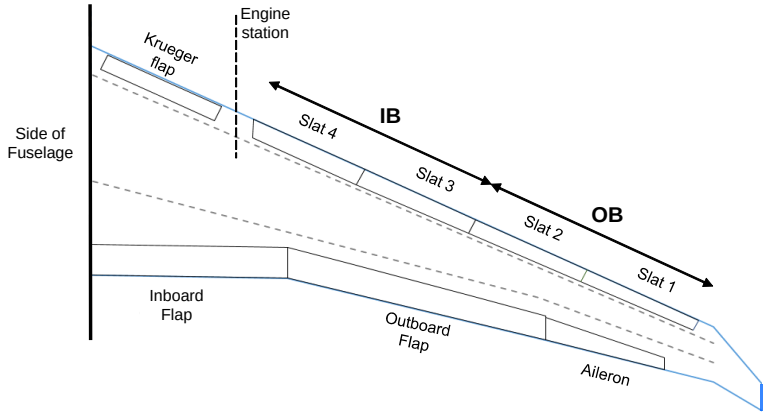

Fig. 2 Schematics of wing leading edge devices.

2. Targeted Applications

Several AFC applications that are described in the following sections are mapped in Fig. 3. The orientation of the jet efflux is also schematically shown for the respective applications. Potential fluidic sources for each of these implementations are also listed. Further details and simulation results are provided in the respective sections.

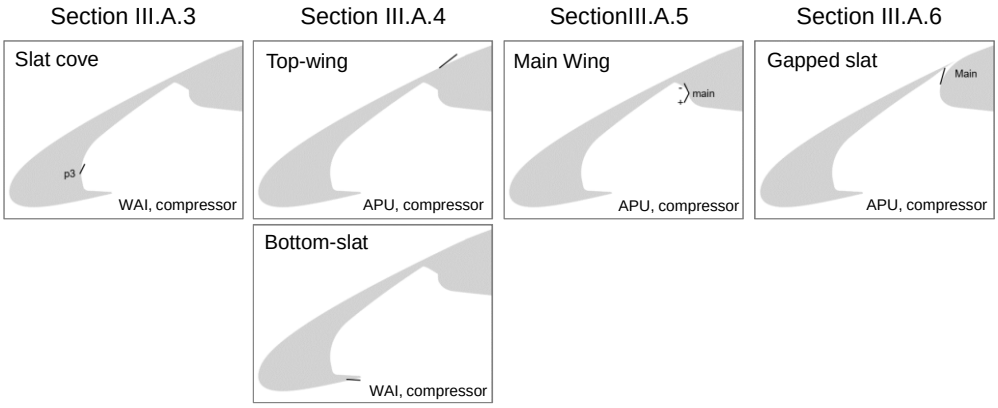

Fig. 3 Targeted AFC applications at the leading edge region.

3. Slat Cove

Flow control is applied in the cove region of the sealed slat for the Reference Aircraft in Fig. 2. AFC is first applied at slats 3 and 4, which are also the slat elements that use WAI. The cove region uses very fine grids to capture the important flow features associated with the recirculation flow and jet interactions. Surface boundary conditions are used on a strip of constant width along the slat span, as illustrated in Fig. 4. In this section, the jet is applied at the vertical portion of the cove surface, which is the forward part of the cove. The jet is discretized by 40 and 136 cells in the xz and the spanwise direction, respectively. The grid consists of 98 million cells and 214 subzones. The jet angle is specified and AFC intensity is determined by PR and TR. All the results presented here use TR=1. The freestream Mach number is 0.20 and Re=6 million based on mean aerodynamic chord. This Reynolds number is consistent with that used for the majority of the computational simulations in the companion paper on the aileron AFC applications

[5]. The nominal angle of attack at takeoff is 6°. Figure 4 shows the Mach number contours on a vertical cut for the baseline and the actuated cases obtained for the nominal takeoff angle of attack of 6°. The baseline case indicates the formation of a counterclockwise vortex with a span component. This particular actuation helps suppress the recirculation.

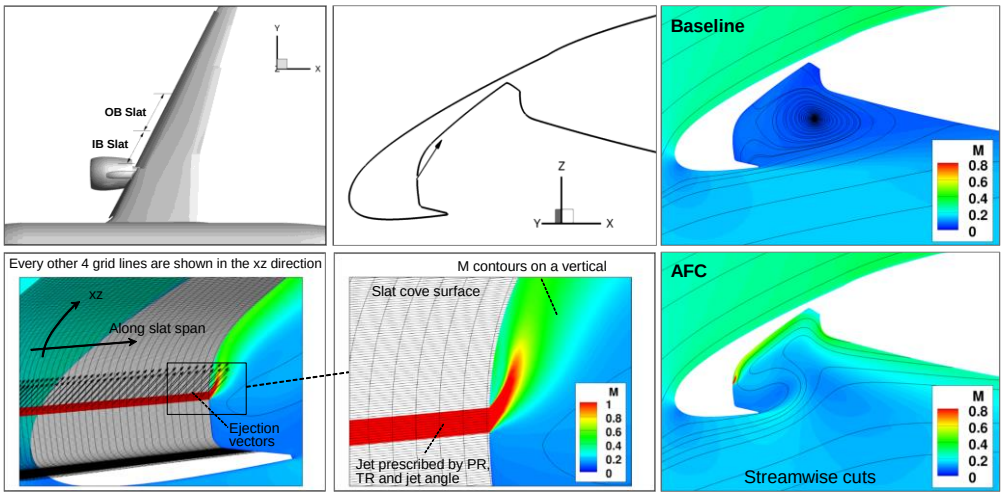

Fig. 4 Modeling approach of AFC in the slat cove.

Figure 5 shows the flow around the airplane in a set of perspective views to help examine the impact of actuation on the flow structure. A set of streamwise cuts show total pressure contours and wing wake development. A packet of streamlines from the slat cove help shed light on the flow patterns at the slats. The simulation indicates that the baseline flow is predominantly three dimensional in the vicinity of the slat, whereby vortical flow forms in the slat cove and it emerges into the ambient stream toward the wing tip. In a sense, the vortex is trapped within the cove. The actuation pattern shown in the inset depicts the ejection vectors that protrude through the transparent outer mold line (OML). The actuation helps break the original counterclockwise flow. This helps curb spanwise flow in the cove region and reduces 3D effects. The streamlines indicate that the actuation promotes faster mixing of the cove stream with the surrounding flow. The intensity of the trailing vortex is thereby reduced, hence resulting in lower airplane drag.

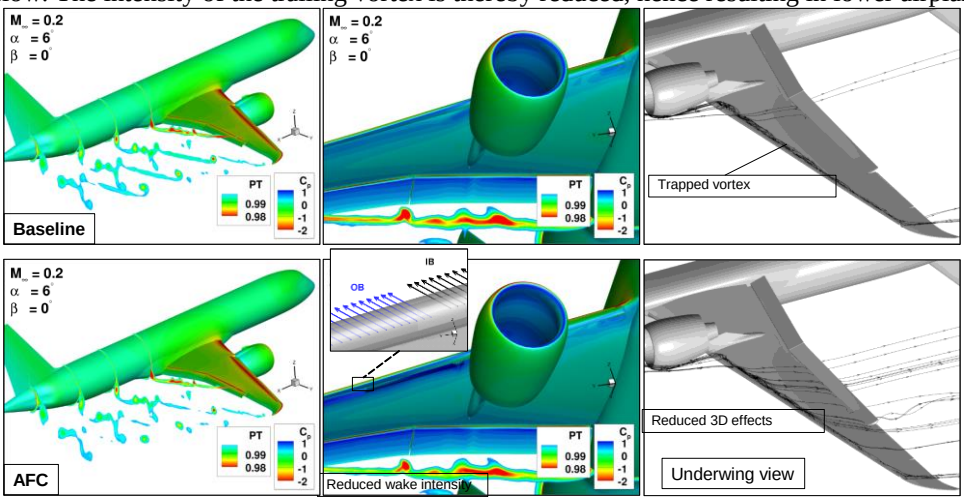

Fig. 5 Impact of slat cove AFC on airplane flow structure.

The first round of simulations uses actuation in the coves of slats 4 and 3, or in the IB and OB segments per the notation of the planform inset in Fig. 4, respectively. A set of simulations were obtained for various jet angles and jet layouts. These results are not included here but a concise summary is presented in Fig. 6 in terms of L/D improvement as a function of actuation mass flow. These flow control patterns are based on 'xy20', where the jet is at 20° off the surface and it points toward the tip of the wing. In addition to the first three patterns, two other layouts are included. In the 'xy20 IB Midx2', the jet is applied at the center of the IB slat element over 25% of its span. The 'xy20 IB Mid Thin' layout denotes a jet applied at the center of the IB over 50% of its span, and it is half the jet width used in all

the other xy20 patterns. The results indicate that only the smaller jets of these last two layouts require mass flow within the limits of an equivalent APU, producing less than 1% improvement in L/D. Figure 7 shows the aerodynamic characteristics of some of the patterns.

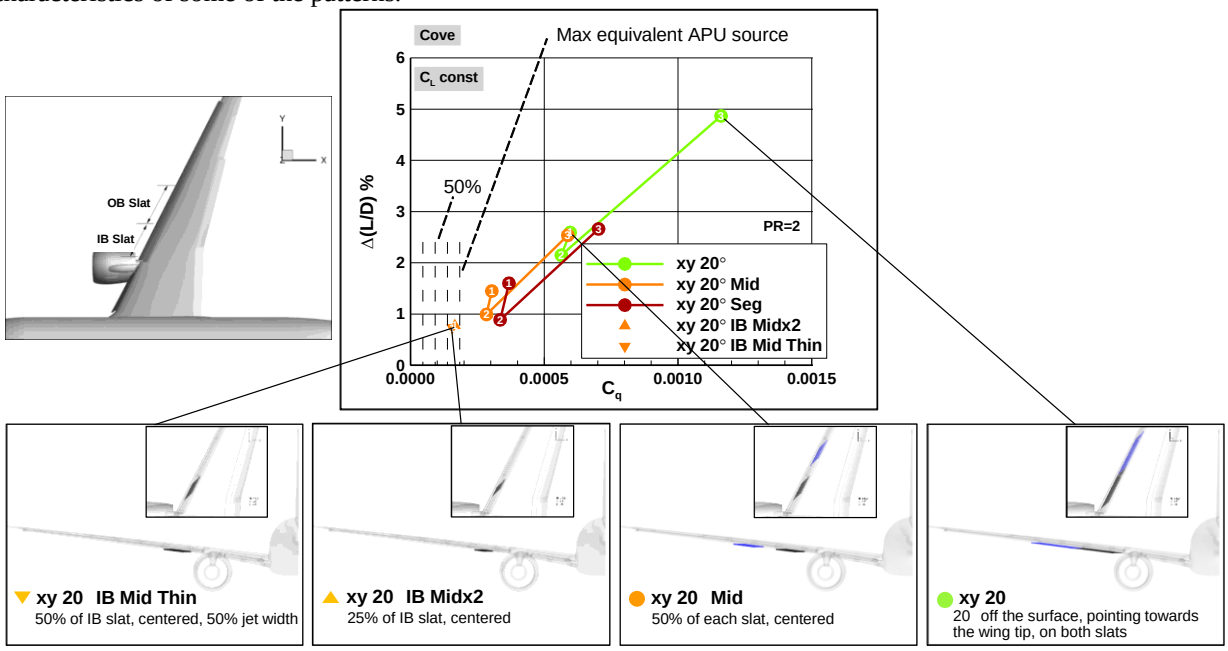

Fig. 6 L/D gains due to actuation in the slat cove.

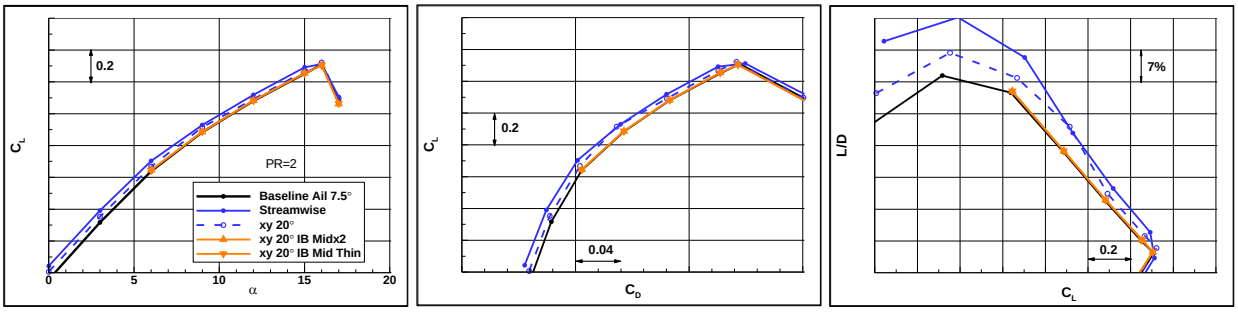

Fig. 7 Effect of slat cove actuation on the aerodynamic performance.

4. Top-Wing/Bottom-Slat

Other possible applications of AFC might be considered. For example, actuation on the top of the wing or in the wing under-slat surface (WUSS), so that the actuator exit is concealed within the OML during cruise. Potential sources are APU or local compressors. Another potential application of AFC is at the lower surface of the slat where the air from the WAI system is exhausted into the freestream. Pressurization of this air could be exploited for flow control if proven aerodynamically beneficial. These two application types are denoted 'Top-wing' and 'Bottom-slat'. Sample solutions are shown in Fig. 8 with actuation on all the slat elements, based on the convention in Fig. 2, where IB consists of slats 3 and 4, and OB includes slats 1 and 2. The L/D gains due to the 'Top-wing' and 'Bottom-slat' are shown in Figs. 9 and 10, respectively. Flow control patterns marked 'Mid' denote a jet centered at the midspan of the slat, spanning 50% of its length. Also, the jets have a fixed nominal width, unless marked 'Thin', which signifies a smaller jet width having half the nominal value. The label 'Thinx2' is a jet of one quarter that of the nominal jet width. The actuation intensity of the cases identified by individual symbols corresponds to PR=2. Selected flow control patterns were obtained at PR=2 and 4, in which cases are identified by a solid line. Generally, actuation at the OB section is more effective than IB, for both the 'Top-wing' and 'Bottom-slat' modes. Also, 'Top-wing' is more effective than 'Bottom-slat'. This is conveniently inferred from Fig. 11, which groups the cases from Figs. 9 and 10 into the black and blue family of symbols, respectively. Based on these results and assuming a maximum allowable mass flow level of an APU (the right most vertical dashed line), the following conclusions can be drawn. The 'Bottom-slat'

pattern ‘AFC Bot OB Mid Thin’ produces an L/D gain of about 1% at PR~1.5. The ‘Top-wing’ actuation ‘AFC Top OB Mid Thin’ with PR~2.5 results in 3% improvement in L/D.

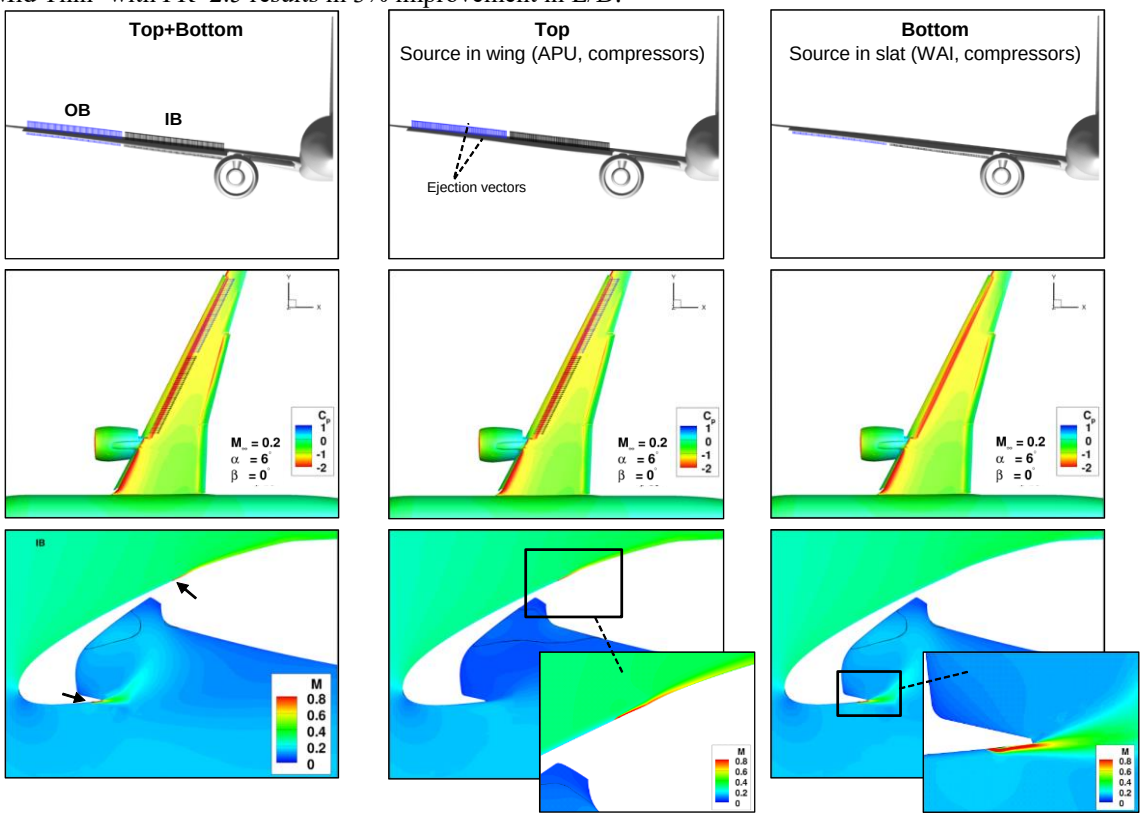

Fig. 8 Top-wing, Bottom-slat and combined Top-wing/Bottom-slat applications.

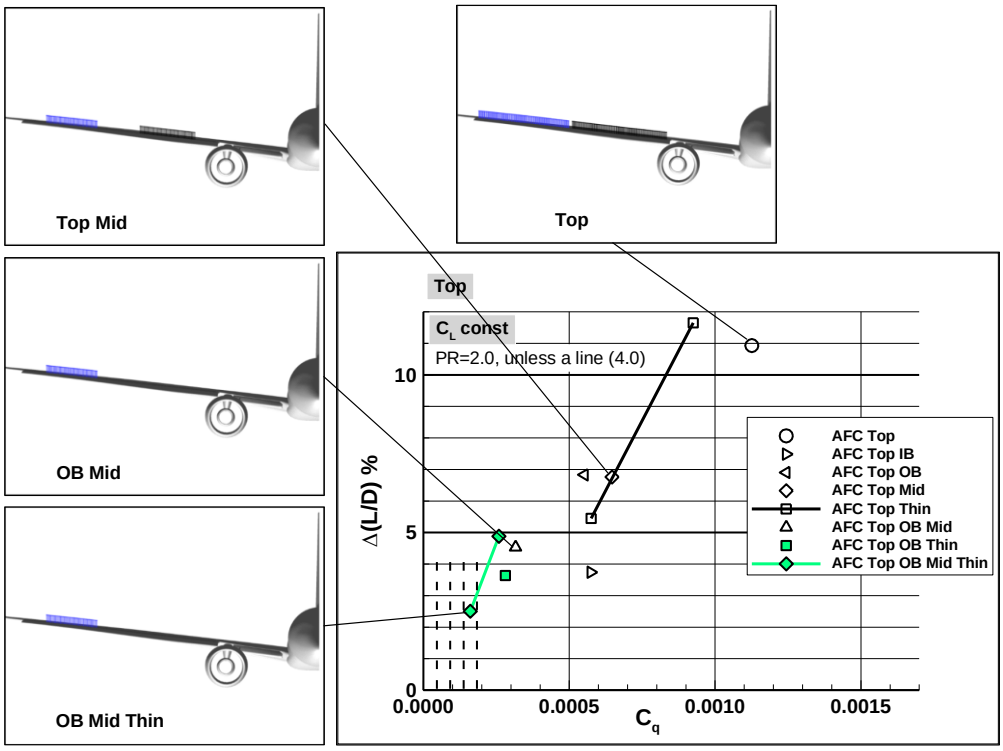

Fig. 9 L/D improvements due to AFC at the top wing.

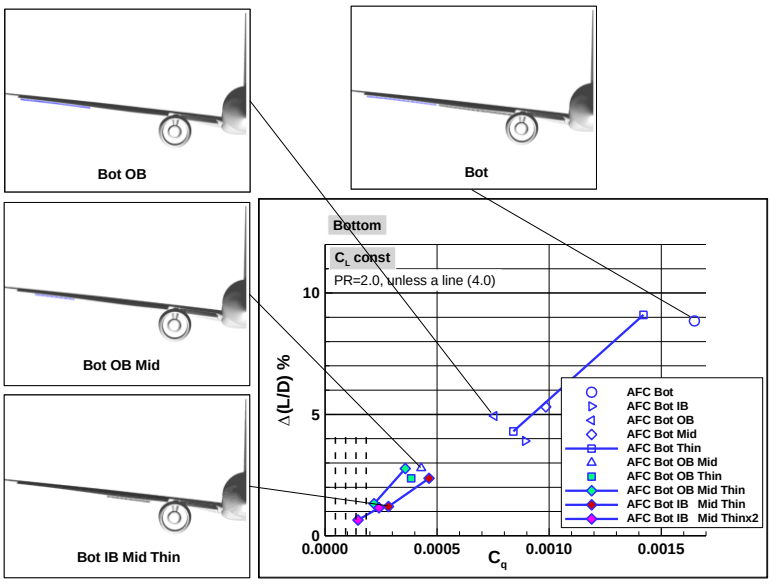

Fig. 10 L/D improvement due to AFC at the bottom slat.

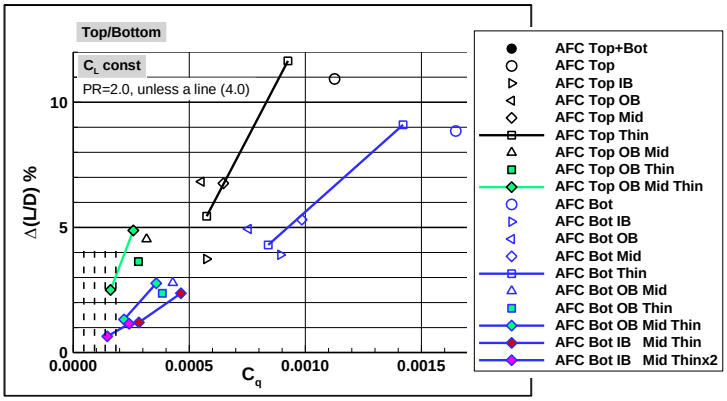

Fig. 11 L/D improvement due to combined top wing/bottom slat application.

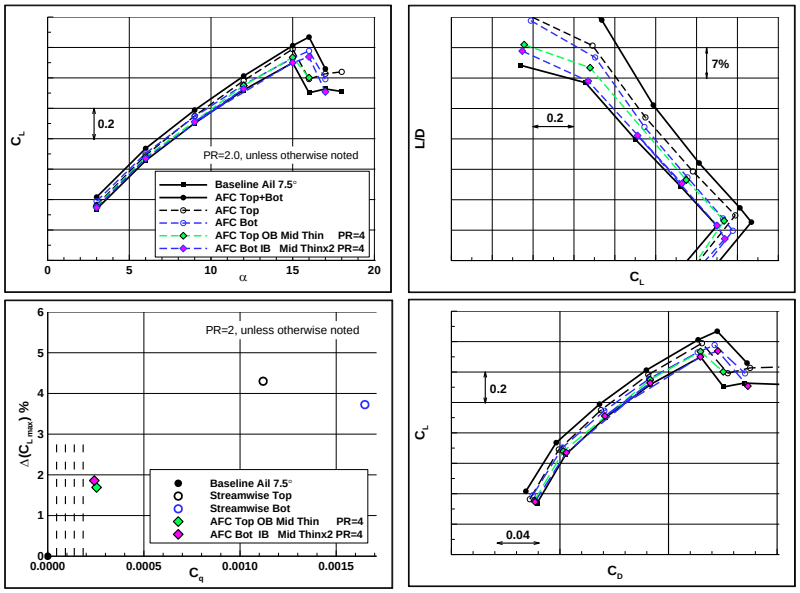

Fig. 12 Aerodynamic performance due to selected AFC applications from Figs. 9 – 11.

The aerodynamic performance of some of the actuation patterns are shown Fig. 12. Aside from the potential for higher L/D, there is also a benefit in maximum lift, which is also presented in terms of percentage improvement as a function of actuation input level.

5. Main Wing

Actuation is applied in the slat cove but at the main wing element. Potential fluidic sources are APU and local compressors. Figure 13 presents the flow fields in the cove region in the midsection cuts of the IB and OB segments. The jet angle is at about 40° angle to the surface. The jets are applied in the clockwise and counterclockwise directions, and denoted 'p' and 'm', respectively. The nominal jet width is identical in both cases. These solutions are shown in the two columns on the left-hand side of Fig. 13. The L/D gains are shown in Fig. 14. The plot includes solutions obtained for thinner jets, having 50% of the nominal jet size. These smaller jets are marked 'p Thin' and 'm Thin'. Although the clockwise oriented jets are slightly more effective, none of these jet patterns offer benefits in the practical mass flow range. For a more effective Coanda effect in the LE region where surface curvature is relatively high, a shallower angle of about 30° was also applied to the clockwise jet. This pattern is shown in the right column in Fig. 13 and it is dubbed 'p Ang-10'. The L/D gains for a set of patterns are shown in Fig. 15, demonstrating that refinements in jet layout may yield significant improvements. There is high dependency on jet angle and span location. Jets with smaller surface angles are more effective. Also, outboard placement of the jets is more advantageous, similar to the findings in Section III.A.4. Nevertheless, the main wing application produces modest gains in L/D. The aerodynamic performance obtained with actuation at the wing is shown in Fig. 16 for selected jet patterns, indicating no improvement in maximum lift.

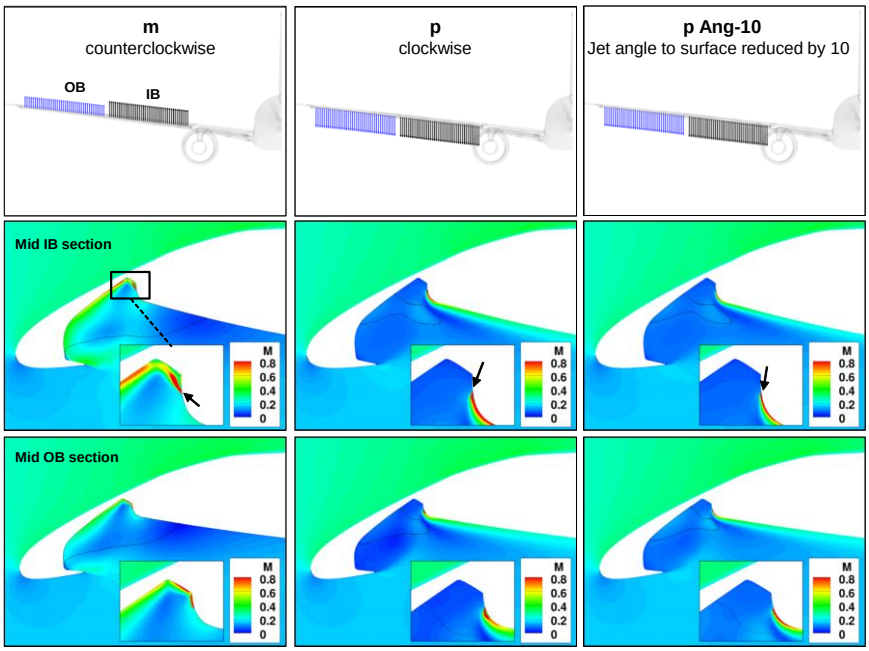

Fig. 13 Main wing applications.

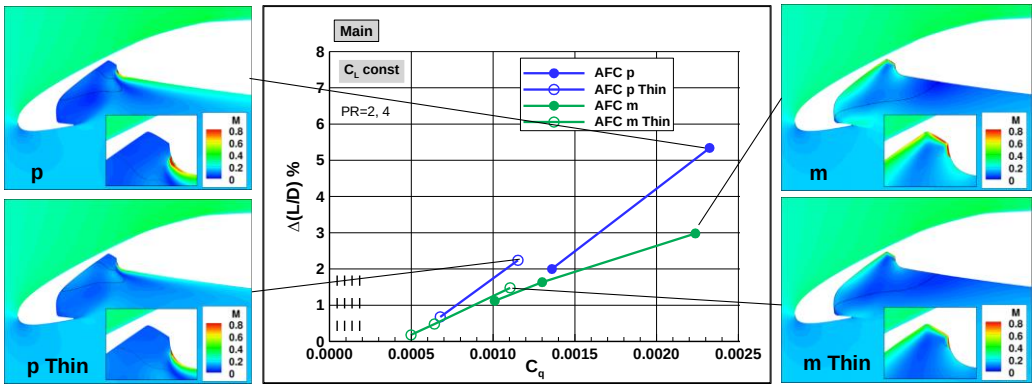

Fig. 14 L/D due to AFC at the wing.

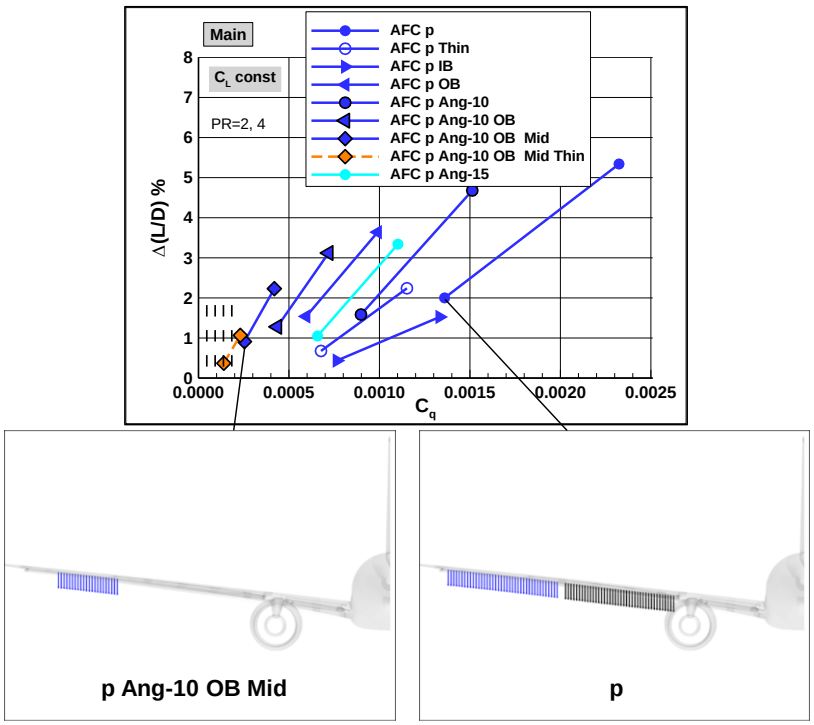

Fig. 15 L/D improvements due to AFC at the wing for various jet patterns.

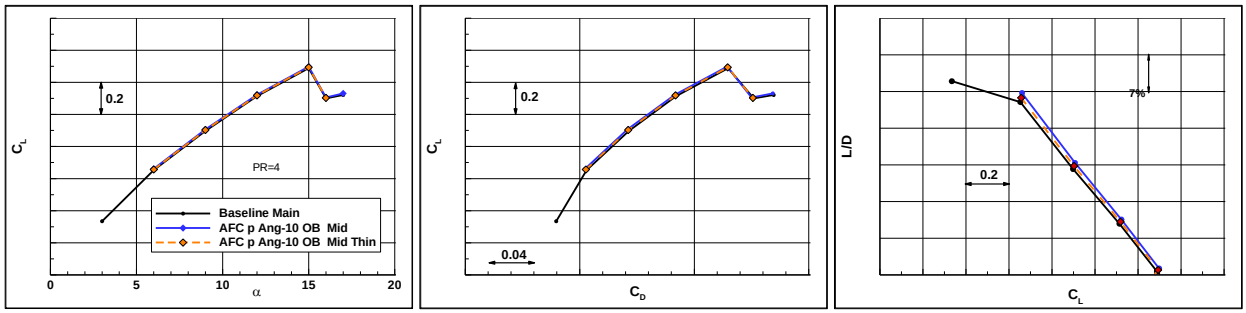

Fig. 16 Aerodynamic performance due to AFC on the wing for selected AFC applications from Fig. 15.

6. Gapped Slat

This flow control approach was conceived from the 'Top-wing' (Section III.A.4) and 'Main wing' (Section III.A.5) applications. For convenience, the Mach number distributions at a spanwise cut in the LE region obtained with these two approaches are presented in Fig. 17. The gapped slat variant is obtained by introducing a small gap between the slat and main wing. The flow control is provided by a jet similar to the one shown in the 'Main wing' inset. Here, the jet is injected at a ~20° angle to the surface toward the throat section. Essentially, the gap creates an effective converging nozzle, so that the jet emerges over the upper surface of the wing, similar to the jet ejection in the 'Top-wing' case. The converged nozzle helps accelerate the jet to higher velocity, thus providing high momentum and amplifying flow control effectiveness. In yet another variant, also included in Fig. 17, the gap is designed to create an effective convergent/divergent nozzle so that the jet can be accelerated to supersonic flow for even higher momentum. The convergent/divergent gap is used in the following results. The gapped slat application can be powered by either APU or local compressors.

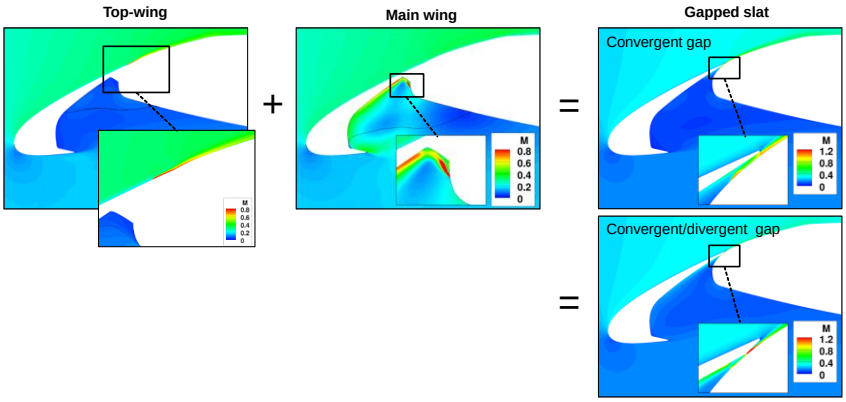

Fig. 17 Gapped slat layout is obtained from the combination of the Top-wing and Main-wing approaches.

The CFD model for the gapped slat is shown in Fig. 18. The slat is at the same detent as in the original sealed position in order to preserve the general aerodynamic characteristics of the original wing. For the purpose of this analysis, the slat lower surface is modified to incorporate a convergent/divergent section. The nozzle area ratios determine the jet velocity as it exits the gap. The diffuser section has an angle of 7.5° to help prevent local flow separation. The wing surface was not modified. It is noted that the gapped slat system uses very small gaps and the slats are at the takeoff detent, and it should not be confused with the slotted (sometimes referred to as gapped) slats used at landing.

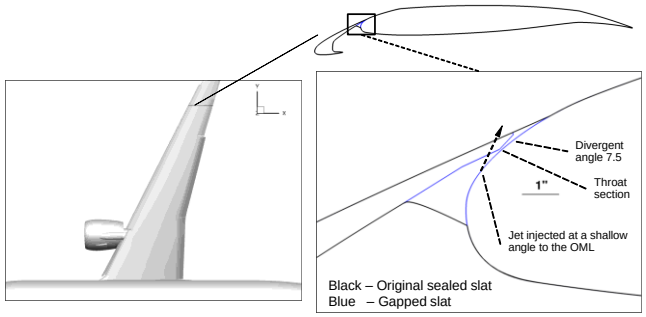

Fig. 18 Gapped slat geometry for the CFD model.

An optional implementation of a gapped slat system on the airplane is shown in Fig. 19. Here the wing has alternate span segments that incorporate very shallow indentations in the WUSS. When the slat is in the sealed position, the indented sections become gapped and the nonindented sections become sealed. In other words, in the sealed slat mode, the indentations form a set of nozzles from which the jets are ejected on the upper surface. When the slats are retracted, the indentations are completely hidden and the cruise mold lines are not affected. Another implementation might use indentations on the lower slat surface.

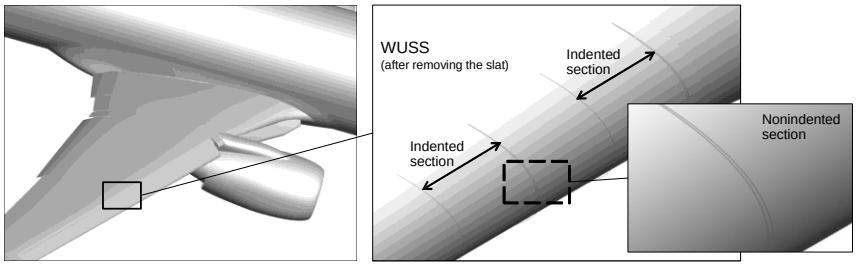

Fig. 19 Gapped slat implementation.

In the first round of CFD simulations, a single grid system was used with gaps at the four slat elements (see Fig. 2). A systematic analysis revealed that the outboard slat (slat 1) was the most effective. However, applying AFC only on a single slat rendered the nonactuated slats effectively unsealed (open gaps). This has resulted in maximum lift degradation. Therefore, a new grid system was developed where only slat 1 incorporates the gap, at the wing segment where actuation is applied. The results with the gapped outboard slat are presented next.

Figure 20 shows the solutions for several AFC layouts. The actuations with PR=2 and 4 clearly show that the jets are diffused right after leaving the wing surface, but accelerate to sonic velocities at the throat section, and further to supersonic velocities in the divergent section of the gap. The actuation produces a thin film of high momentum that remains attached to the upper wing surface. The difference in the flow development on the upper surface between the two jet intensities is evident. The effect of jet location relative to the throat section is shown in the third column from the left. Relative to the original location, the jet was placed further downstream and closer to the throat. This actuation uses PR=2 and it is denoted 'OB Dns'. Relative to the original jet location (first column), 'OB Dns' results in higher velocities in the diffuser and further over the upper surface of the wing. The fourth column presents a case in which the original PR=2 actuation is limited to just the outboard half of the slat, labeled 'OB ob'.

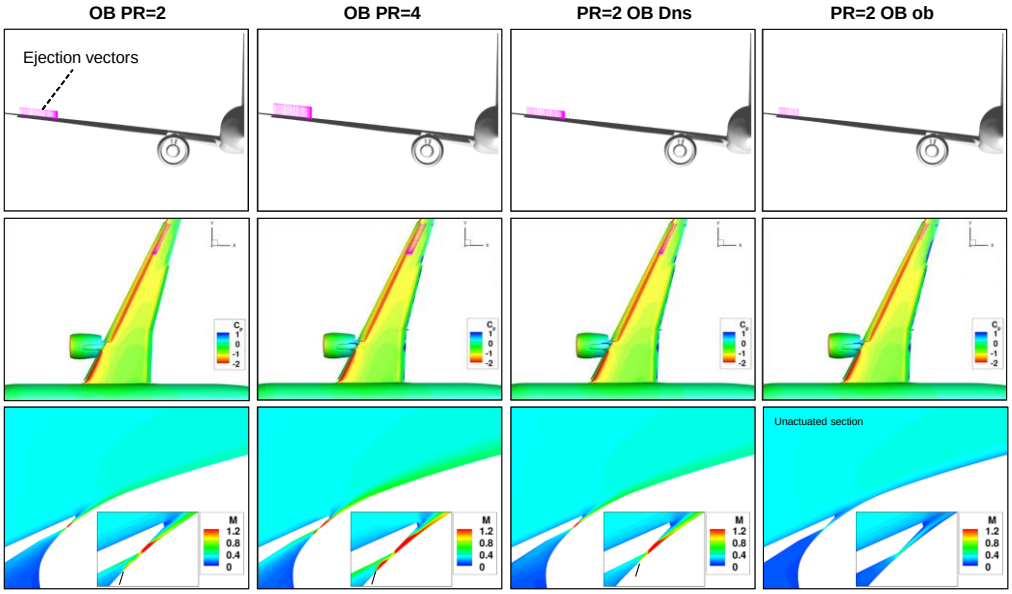

Fig. 20 Selected gapped slat applications on the outboard slat (slat 1).

The improvements in L/D are presented in Fig. 21 for the patterns described above and several additional variants. 'OB Ups' denotes a jet that is placed further upstream relative to the original location in the first column in Fig. 20. 'OB ib' uses actuation in the inboard half segment of the outboard slat. 'OB ob wide' is a jet with twice the width of actuation as 'OB ob'. First, it is noted that the gapped slat with no actuation helps gain about 0.3% in L/D. Using a set of PRs of 1.6, 2 and 4, several of the patterns land in the practical range of mass flow that could be supplied by the APU. In terms of jet placement, the closer to the throat area the jet is, the more effective the actuation. For example, at PR=1.6, 'OB Ups' results in 1% increase in L/D, 'OB' in 1.5% and 'OB Dns' in 2%. Actuation on the outboard part of the slat 'OB ob' is more effective than the inboard segment 'OB ib'. Finally, the wider jet does not yield higher actuation efficiency. An increase of about 2.7% in L/D is achievable with several jet configurations at various pressure levels and within the APU limits. Figure 22 shows the aerodynamic performance of several of the patterns, indicating that the original C_{Lmax} is preserved.

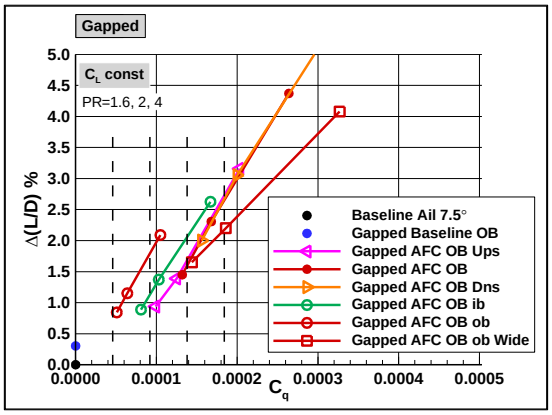

Fig. 21 L/D improvement due to gapped outboard slat.

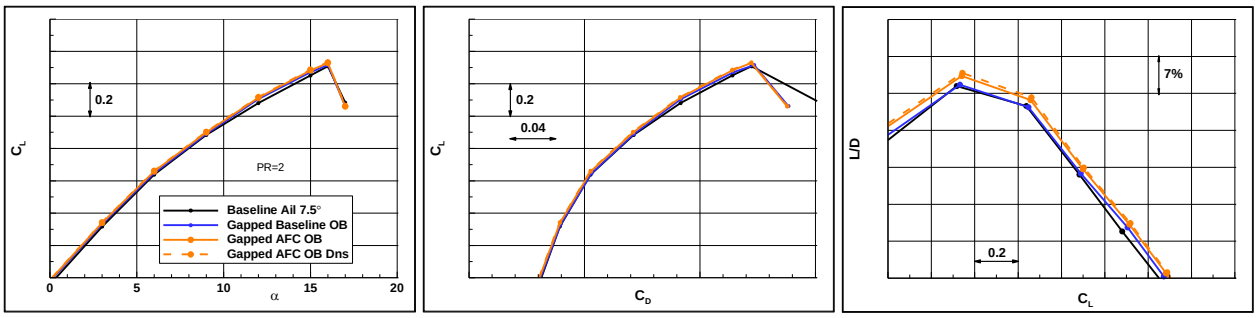

Fig. 22 Aerodynamic performance due to gapped outboard slat.

At this point, it becomes obvious that the 'Top-wing' actuation and the 'Gapped-slat' produce similar results. Although there are different aspects of integration of such systems, it is instructive to compare their aerodynamic performance. This is presented in Fig. 23. It is noted that this is merely a comparison of results obtained for two AFC approaches and there was no attempt to implement the flow control in a consistent manner. For example, the jet width and the jet angle to the local surface are different. Nevertheless, the trends in L/D appear to be quite similar with measurable L/D improvement in the practical C_q range. It is interesting that the relative benefits between the two implementations switch as actuation is placed closer to the wing tip. 'Top-wing' is more effective when actuation is applied on the entire outboard slat (OB), whereas the advantage flips over to the 'Gapped-slat' when the actuation is confined to the outboard segment of the slat (OB ob). This implies that further gains could be realized by refining these initial implementations in both actuation approaches.

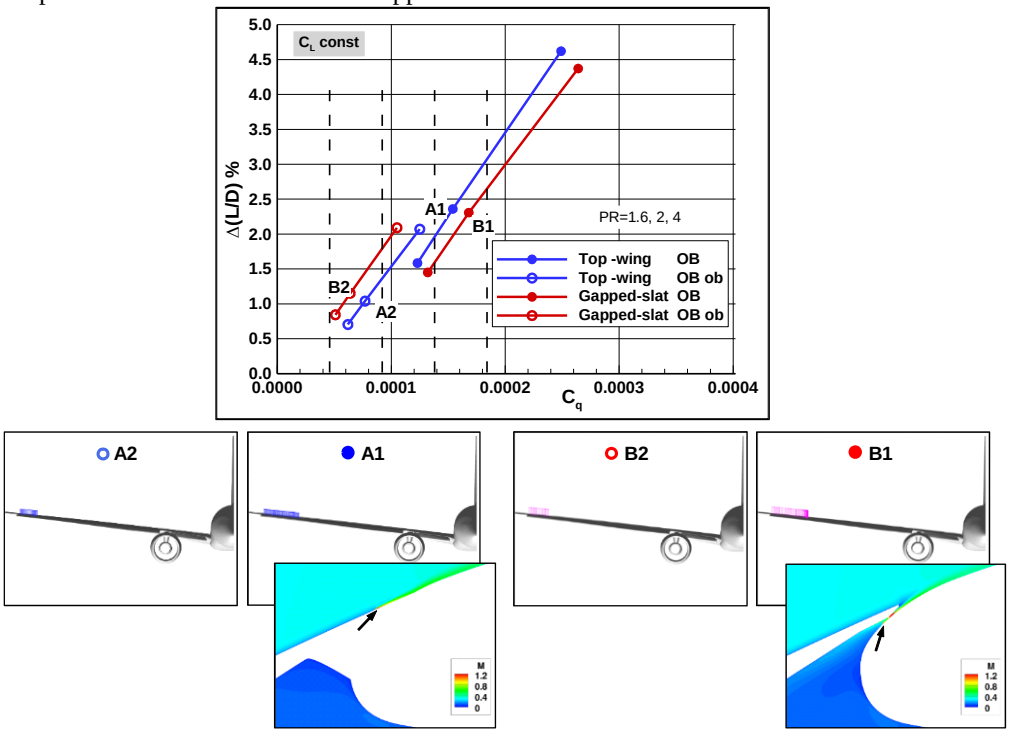

Fig. 23 Aerodynamic performance of Top-wing and Gapped-slat at the outboard slat element.

B. AFC in Nacelle/Pylon/Wing Region

The integration of the engine installation with the wing high-lift system introduces interference effects that adversely impact the airplane performance during low speed operations. AFC was applied in the general wing/pylon region in order to alleviate the aerodynamic shortcomings and improve performance over the range of angles of attack, including C_{Lmax}. This problem is especially important for the integration of very high-bypass-ratio engines of future airplanes. In addition to the potential to enhance aerodynamic performance, AFC may enable simpler integration of the high-lift system with the pylon. Reduced complexity of this mechanical system may result in lower weight and maintenance costs [20].

1. Effect of AFC on the Flow Structure

The flow control layout used for this application is shown in Fig. 24 together with the baseline flow at the nominal takeoff condition of α=6°. The inboard Krueger flap and the outboard slats are sealed. The flow features of the baseline can be seen from the cross-sectional cuts of total pressure contours. Three vortex elements form at the chine, the inboard side of the pylon and the inboard edge of the sealed slat. A very fine mesh was introduced on the fixed wing element in the pylon region for representing small width jets using surface boundary conditions. The flow control is applied on both sides of pylon station as indicated by the color-coded efflux vectors, representing nominal sized jets. The jets lie in the xz plane at the same nominal angle. The results for the baseline and the actuated flows with PR=4 are shown in Figs. 25 and 26 for the flows at α=6° and 16°, respectively, the latter representing near C_{Lmax} conditions. At α=6°, the intensity of vortex elements is substantially reduced by actuation. As the flow incidence increases, flow separation originates at the slat edge, developing into a sizeable bubble at α=16°. The momentum provided by flow control helps suppress the separation and improve the flow quality over this wing segment.

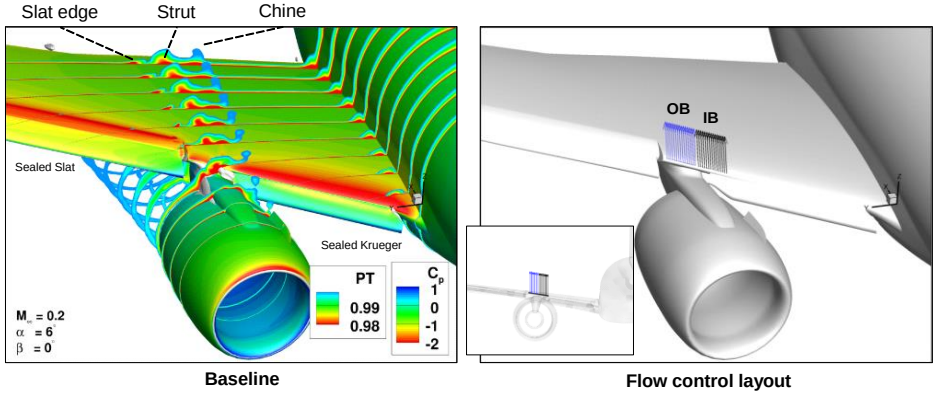

Fig. 24 AFC for improved nacelle/pylon/wing integration.

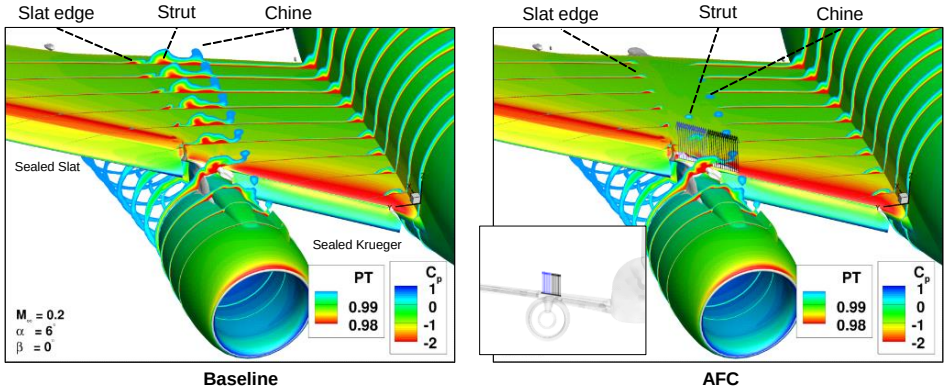

Fig. 25 AFC effect at nacelle/pylon/wing, α=6°.

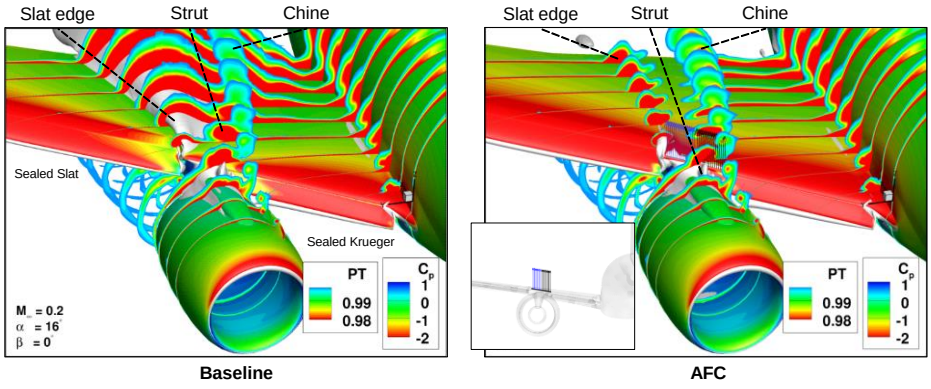

Fig. 26 AFC effect at nacelle/pylon/wing, α=16°.

2. Sensitivity to AFC Patterns

Figure 27 shows flow fields obtained at α=6° for a set of AFC layouts with PR=4. Spanwise cuts on either side of the pylon are also presented. The inboard section is a cut through the sealed Krueger flap and the outboard cut slices through the sealed slat. The two columns on the left-hand side are the cases shown in Fig. 25. The 'Mid' and 'Midx2' notations signify jets whose span lengths are 25% and 50% of the size of the nominal jets. Because of the relatively high surface curvature in the area where flow control is applied, the effects of shallower jet angles were also assessed. The jets marked 'Ang -15' indicate jets having an angle that is smaller by 15 degrees relative to the nominal orientation. Clearly the smaller angle causes the jets to attach quicker to the surface, thereby reducing the tendency of flow recirculation immediately downstream at the foot of the jets. The gains in aerodynamic performance due to AFC is shown in Fig. 28. Results indicate that the smaller jet angle is more effective. Additionally, the outboard actuation patterns (OB) are much more effective than the inboard counterparts (IB) as they avert the formation of the separation at the slat edge, especially in terms of maximum lift. Relative to the applications in previous sections, the gains in C_{Lmax} due to AFC at the nacelle/pylon/wing are substantial, but the improvement in L/D is fairly modest.

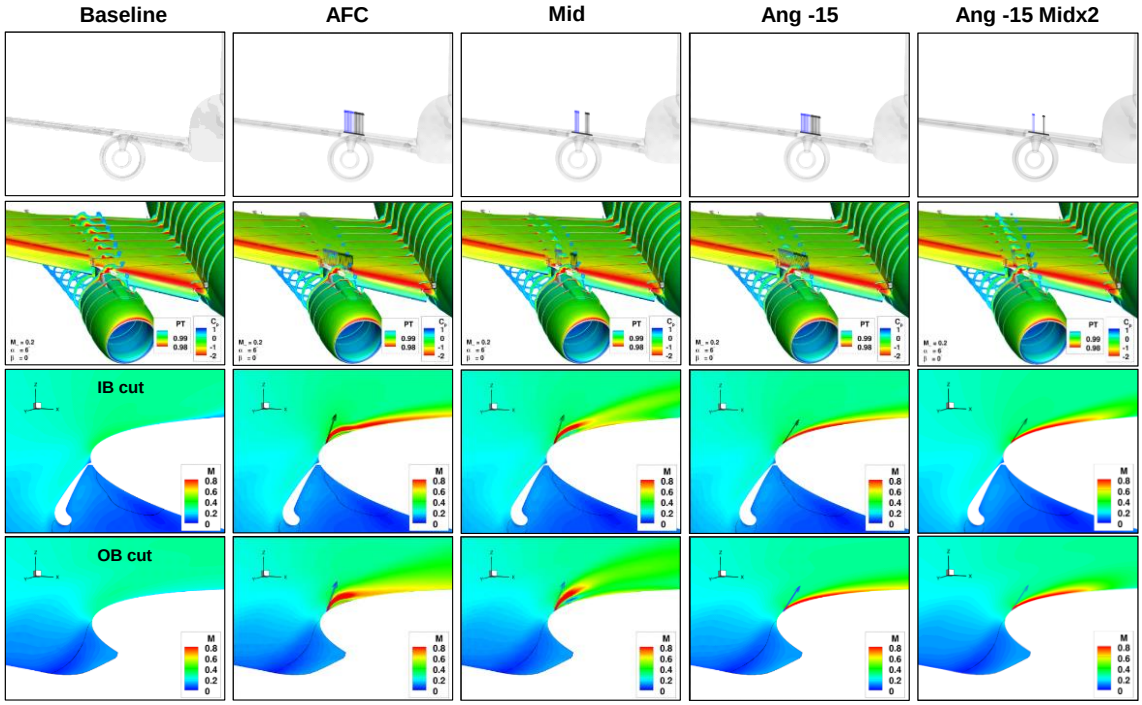

Fig. 27 AFC patterns for the nacelle/pylon/wing application, α=6°.

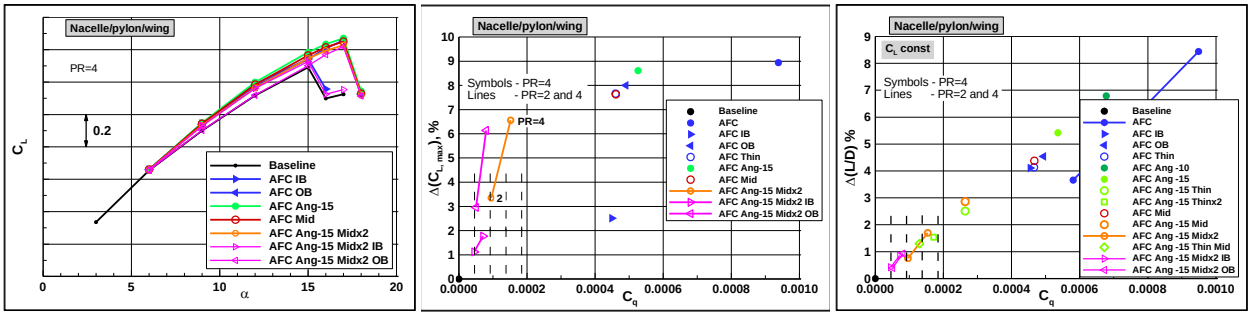

Fig. 28 Aerodynamic performance due to AFC at the nacelle/pylon/wing.

The separation progression for the baseline and the 'Ang -15 Midx2' flow control pattern with PR=4 is shown in Fig. 29. The baseline flow indicates loss of lift at α=16° due to the separation originating at the slat edge whereas the controlled flow outright suppresses this flow feature. Instead, the critical separation points occur at α=18° and they shift to the leeward side of the engine cowl and the inboard section of the wing that is protected by the Krueger flap.

Figure 30 illustrates the difference between inboard vs outboard actuation with the 'Ang -15 Midx2' pattern and PR=4. Clearly the outboard actuation is most effective in preventing separation, commensurate with the aerodynamic

characteristics in Fig. 28. In fact, there is no material benefit in using the inboard actuation for either L/D or C_{Lmax} improvements for this flow condition. However, inboard actuation improves C_L in the linear range. Examination of the flow structure at α=15° in the top views of the baseline (Fig. 29), the IB and OB actuation cases (Fig. 30) reveal that the flow quality in the inboard wing section has improved with IB actuation, and the separation pocket at the trailing edge flap is reduced. However, beyond α=15°, the separation off of the slat edge dominates the flow and stall ensues.

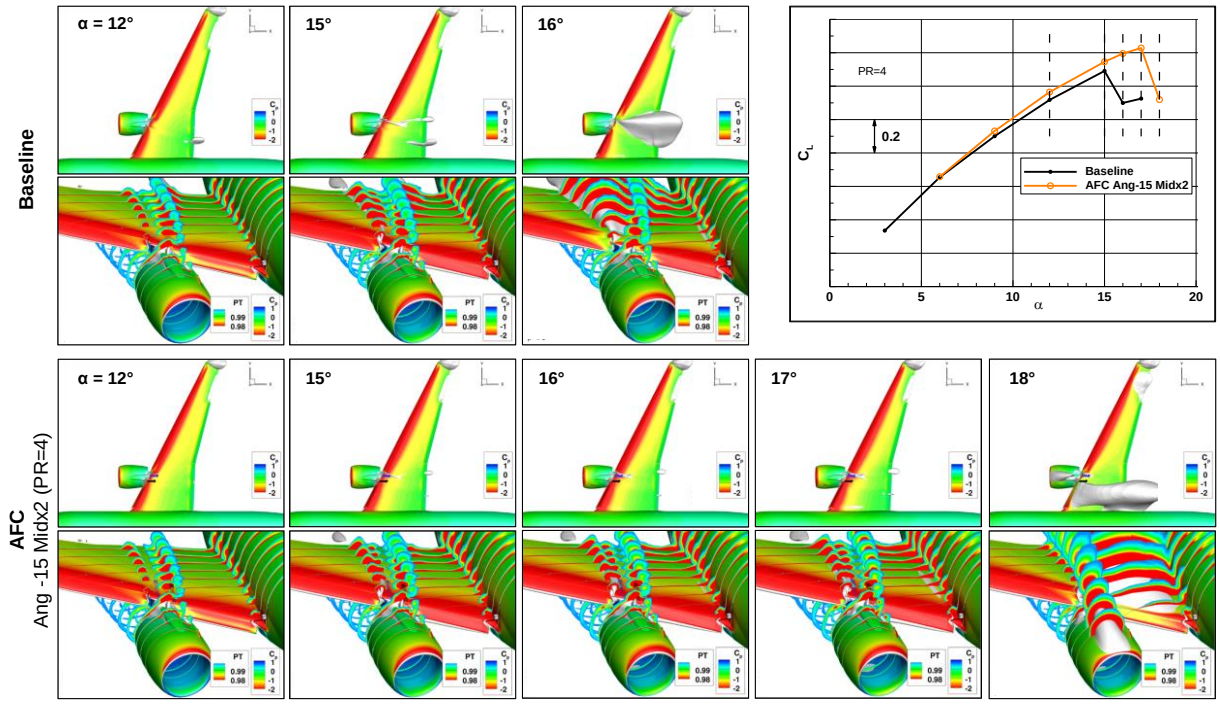

Fig. 29 Flow development with angle of attack for the baseline and the Ang -15 Midx2 pattern with PR=4.

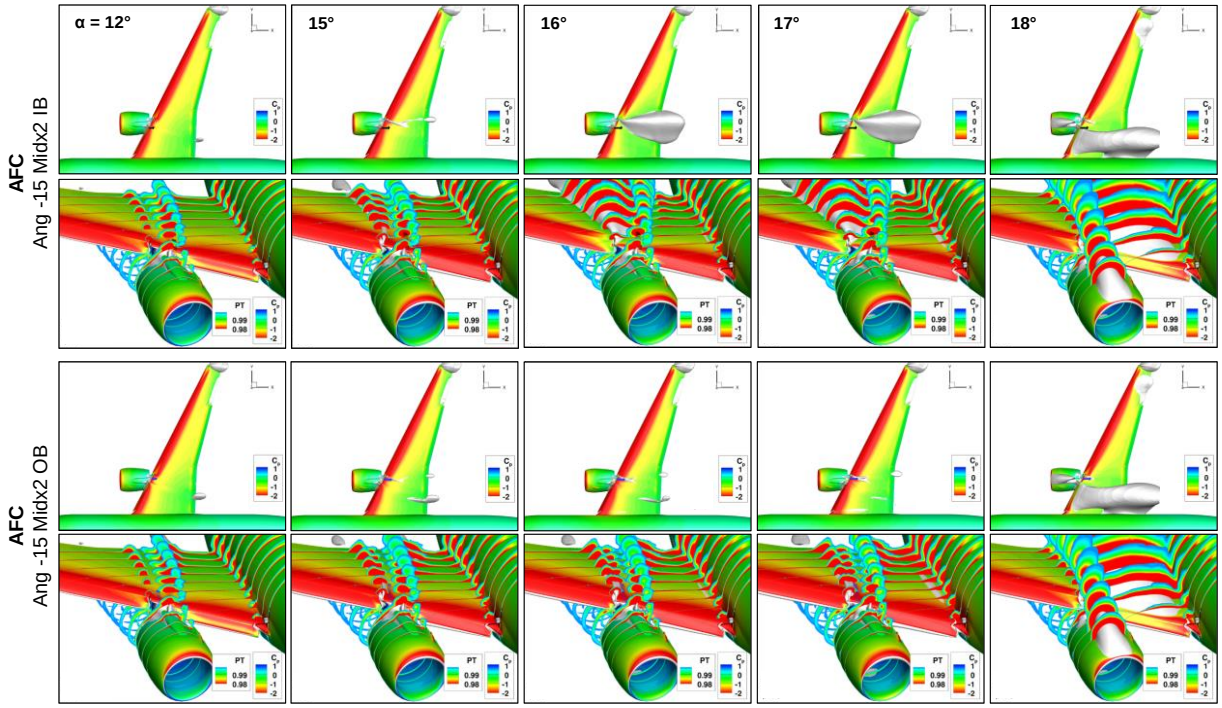

Fig. 30 Flow development with angle of attack for the inboard and outboard actuation, Ang -15 Midx2 patterns with PR=4.

IV. Conclusions

Flow control approaches targeting the leading edge regions of the wing of a commercial airplane at high-lift conditions were investigated. The first class of flow control applications targets various locations in the wing leading edge regions, including the slats and the wing element. Depending on the specific applications, the objective is to reduce viscous effects and to control the vortical flow. The increase in lift, including C_{Lmax}, and the reduction in drag result in improved L/D during takeoff, which is a major determinant of airplane performance. The improvements in L/D are of the order of 1-2% if considering available air sources on the aircraft.

The other flow control approach is aimed at reducing the interference effects and facilitating the integration of the engine with the wing high-lift system, a critical element in the integration of very high-bypass-ratio engines of future airplanes. Here, the primary objective is to control the associated vortex system in order to enhance lift up to stall and beyond. The results suggest that more than 5% increase in C_{Lmax} and a delay in stall angle by 2° are achievable. The AFC methods were designed for the least amount of actuation input in order to enable practical integration using onboard sources.

Acknowledgements

This study was sponsored by NASA under Contract NNL16AA04B-80LARC20F0082. Dr. John C. Lin and Mrs. Latunia Melton were the NASA Langley Research Center Principal Investigators.

References

1. Hartwich, M.P., Camacho, P., El-Gohary, K., Gonzales, A.B., Lawson, E.L. and Shmilovich, A., "System-Level Trade Studies for Transonic Transports with Active Flow Control (AFC) Enhanced High-Lift Systems," AIAA 2017-0321, DOI: 10.2514/6.2017-0321
2. Shmilovich, A., Yadlin, Y., Dickey, D.E., Hartwich, M.P., & Khodadoust, A., "Development of an Active Flow Control Technique for an Airplane High-Lift Configuration," *AIAA SciTech Forum*, Grapevine, TX, Jan 9-13, 2017, DOI: 10.2514/6.2017-0322
3. Whalen, E.A, Shmilovich, A., Spoor, M., Tran, J., Vijgen, P., Lin, J.C., & Andino, M., "Flight Test of an Active Flow Control Enhanced Vertical Tail", *AIAA Journal*, Vol. 56, No. 9, 2018, DOI: 10.2514/1.J056959
4. Garner, P., Meredith, P., & Stoner, R., "Areas for future CFD development as illustrated by transport aircraft applications", *AIAA 10th Computational Fluid Dynamics Conference*, Honolulu, HI, June 24-26, 1991, DOI: 10.2514/6.1991-1527
5. Shmilovich, A., Yadlin, Y., Vijgen, P., & Woszidlo, R., "Flow Control for Enhanced Aileron Effectiveness on a Commercial Aircraft," *accepted for AIAA SciTech Forum*, National Harbor, MD, Jan 23-27, 2023
6. Shmilovich, A. & Yadlin, Y., "Flow Control for Enhanced Airplane Takeoff Performance", *AIAA SciTech Forum*, Orlando, FL, Jan 6-10, 2020, DOI: 10.2514/6.2020-0784
7. Vijgen, P., Ziebart, A., Shmilovich, A., & Woszidlo, R., "Conceptual Integration Studies of Localized Active Flow Control on the Wing of a Commercial Aircraft," *accepted for AIAA SciTech Forum*, National Harbor, MD, Jan 23-27, 2023
8. Woszidlo, R., Shmilovich, A., & Vijgen, P., "Low-Speed Performance Enhancement using Localized Active Flow Control – Program Overview and Summary", *NASA Technical Reports Server*, April, 2022, document ID: 20220006728
9. Shmilovich, A., Vijgen, P., & Woszidlo, R., "Low-Speed Performance Enhancement using Localized Active Flow Control – Localized Active Flow Control Simulations on a Reference Aircraft", *NASA Technical Reports Server*, April, 2022, document ID: 20220006731
10. Vijgen, P., Ziebart, A., Shmilovich, A., & Woszidlo, R., "Low-Speed Performance Enhancement using Localized Active Flow Control – Integration Study of Localized Active Flow Control on a Performance Reference Aircraft", *NASA Technical Reports Server*, April, 2022, document ID: 20220006733
11. Shmilovich, A., Stauffer, M., Woszidlo, R., Vijgen, P., "Low-Speed Performance Enhancement using Localized Active Flow Control – Simulations, Scaling and Design of Localized Active Flow Control on the Common Research Model", *NASA Technical Reports Server*, April, 2022, document ID: 20220006736
12. Buning, P.G., Chiu, I.T., Obayash, S., Rizk, Y.M., & Steger, J.L., "Numerical Simulation of the Integrated Space Shuttle Vehicle in Ascent", *15th AIAA Atmospheric Flight Mechanics Conference*, Minneapolis, MN, Aug 15-17, 1988, DOI: 10.2514/6.1988-4359

13. Shmilovich, A., & Vatsa, V., "Practical Computational Methods for Airplanes with Flow-Control Systems," *AIAA Journal*, Vol. 57, No 1, 2019, DOI: 10.2514/1.J056876
14. Shmilovich, A., "Unconventional Applications and New Approaches for Flow Control", in *Fundamentals of High Lift for Future Civil Aircraft, Notes on Numerical Fluid Mechanics and Multidisciplinary Design*, Springer book series, Vol. 145, Edited by Radespiel and Semaan, 2020, DOI: 10.1007/978-3-030-52429-6_1
15. Shmilovich, A., Yadlin, Y., & Whalen, E., "Computational Evaluation of Flow Control for Enhanced Control Authority of a Vertical Tail," *AIAA Journal*, Vol. 54, No 8, 2016, DOI: 10.2514/1.J054712
16. Shmilovich, A., Yadlin, Y., & Whalen, E., "Active Flow Control Computations: From a Single Actuator to a Complete Airplane," *AIAA Journal*, Vol. 56, No. 12, 2018, DOI: 10.2514/1.J056307
17. Shmilovich, A., & Yadlin, Y., "Flow Control for the Systematic Buildup of High Lift Systems," *AIAA Journal of Aircraft*, Vol. 45, No. 5, 2008, DOI: 10.2514/1.35327
18. Shmilovich, A., & Whalen, E., "A Technique for Low Input Flow Control Actuation," *35th AIAA Applied Aerodynamics Conference*, Denver, CO, 5-9 June, 2017, DOI: 10.2514/6.2017-3040
19. Shmilovich, A., & Whalen, E., "Strategies for Practical Implementations of Low-Input Thermal Flow Control," *AIAA Scitech Forum*, San Diego, CA, 7-11 Jan, 2019, DOI: 10.2514/6.2019-0886
20. Schloesser, P., Soudakov, V., Bauer, M., & Wild, J., "Active Separation Control at the Pylon-Wing Junction of a Real-Scale Model," *AIAA Journal*, Vol. 57, No. 1, 2019, DOI: 10.2514/1.J057345